Int J Adv Manuf Technol (2018) 95:719–733
https://doi.org/10.1007/s00170-017-1222-0

ORIGINAL ARTICLE

Investigation and modeling of flank wear process of different PCD tools in cutting titanium alloy Ti6Al4V

Guangxian Li[1] · **Nan Li**[1] · **Cuie Wen**[1] · **Songlin Ding**[1]

Received: 5 June 2017 / Accepted: 16 October 2017 / Published online: 2 November 2017

Abstract Owing to its ultra-hardness, polycrystalline diamond (PCD) is ideal for the machining of difficult-to-cut materials. According to ISO 3685, flank wear is the main factor that leads to tool rejections. In this study, a new theoretical model was developed by considering both abrasive and adhesive wear in order to investigate the process and mechanism of flank wear of cutting tools made of different PCD materials. The width of flank wear (VB) was calculated by solving the differential equation formulated to describe the rate of flank wear and its relationship with cutting parameters and the properties of tool and workpiece materials. To validate the analytical model, a series of cutting experiments were conducted by turning titanium alloy Ti6Al4V with customized tools made of three types of PCD materials. Morphological characteristics of worn areas were analyzed after each cutting test to investigate the wear process and mechanism. It was found that the wear mechanisms of three different types of PCD tools were different. Calculation outcomes matched experimental results when tools made of CTB002 and CTB010 were used. Obvious deviation was found when the tool made of CTM302 was used due to the occurrence of large-scale fracture of tool tip in the cutting passes.

✉ Songlin Ding
songlin.ding@rmit.edu.au

Guangxian Li
s3463966@student.rmit.edu.au

Nan Li
s3468780@student.rmit.edu.au

Cuie Wen
cuie.wen@rmit.edu.au

[1] School of Engineering, RMIT University, Mill Park, VIC 3082, Australia

Keywords Polycrystalline diamond (PCD) · Flank wear · Abrasive wear · Adhesive wear · Titanium turning · Wear mechanism

1 Introduction

Titanium alloys are difficult to machine due to their low thermal conductivity (7 W/m.K) and high chemical reactivity [1]. Severe cutting conditions including high temperature and highly abrasive interaction at tool/chip and tool/workpiece interfaces significantly accelerate the rate of tool wear and cause premature tool [2]. Although new approaches have been developed to machine titanium components with nonconventional methods [3], conventional machining is still the mainstream approach in industry because of the risk of thermal residual stress [4, 5]. Owing to the ultra-hardness and excellent thermal conductivity, polycrystalline diamond (PCD) has been gradually used as an advanced tool material in cutting titanium alloys [6, 7]. According to experimental results [8], PCD tools have much longer tool life compared with WC tools in machining Ti6Al4V at high cutting speeds (over 200 m/min). However, the existence of extensive compressive stress, high-speed abrasion, and high temperature at tool/workpiece interface leads to severe tool wear [9]. It has been found that [10] fracture of tool tip, abrasion and abrasion on tool surface, and notching along the cutting edge were the main wear types of PCD tools. According to Li et al. [11], a large scale of spalling occurred on the flank face of PCD tools in milling Ti6Al4V. Based on the experiments of turning Ti6Al4V, da Silva et al. [12] concluded that the adhesion layer formed on the tool surface was partially removed by "plucking action." Among the different types of tool wear, flank wear, which is caused by the tool/workpiece abrasion, is one of the most important indexes that determines the life of a cutting

tool [13]. Generally, the development of flank wear consists of three stages: the initial wear process, the steady wear process, and the intensive wear process [14]. As shown in Fig. 1, the change of the width of flank wear (VB), i.e., the development of tool wear, indicates the effective tool life of cutting tools.

In order to describe the relationship between tool life and cutting parameters, Taylor proposed an empirical model to define the exponential relationship between tool life and cutting speed [15]. A modified model which defined tool life as a function of cutting temperature was later proposed by Takeyama and Murata [16]. Analytical models which take into account different types of tool wear mechanisms and the missed material properties have been developed [17]. For example, the analytical models proposed by Rabinowicz were widely used when the tool suffered from different types of abrasive wear: two-body abrasion and three-body abrasion [18]. Bhattacharya et al. proposed a wear model considering the effect of adhesion [19]. In this model, the definition of "temperature-sensitive zone" (TSZ) and "temperature-insensitive zone" (TIZ) was proposed. In the tool wear model developed by Choudhury et al. [20], the development of tool wear in turning processes was described mathematically by using parameters including index of diffusion, wear coefficient, and the tool/workpiece hardness ratio. By considering the combination of abrasive wear and adhesive wear, Wong et al. [21] developed an empirical model based on the assumption that adhesive wear was the predominant wear type for flank wear. With the development of synthetic materials, new models were developed to investigate the wear process of ceramic tools, polycrystalline cubic boron nitride (PCBN) tools, and PCD tools. For example, Dawson and Kurfess reported a model of the development of flank wear for uncoated and coated PCBN tools [22]. Similarly, Huang et al. developed a model considering the adhesion as the main mechanism for the flank wear process of the PCBN tools, which was validated by cutting AISI 52100 bearing steel [23].

PCD is a synthetic material made by diamond grains and binder materials under high pressure and high temperature. The mechanical properties of PCD vary significantly owing to the different sizes of diamond particles and the different proportion of binding materials. The significant difference in material properties results in a dramatic difference in the fracture of the polycrystalline structure in micro-scale, and leads to different wear processes and mechanisms in macro-scale. However, to the authors' best knowledge, in addition to some experiment-based investigations, no theoretical model has been created to describe the flank wear process of different PCD tools, and little research has been conducted to investigate the different wear mechanisms and processes of PCD tools caused by different material properties. Since the wear of PCD materials is a complicated process, it is insufficient to limit the research to experimental analysis only; theoretical studies are critical for the in-depth understanding of the wear mechanism of PCD tools.

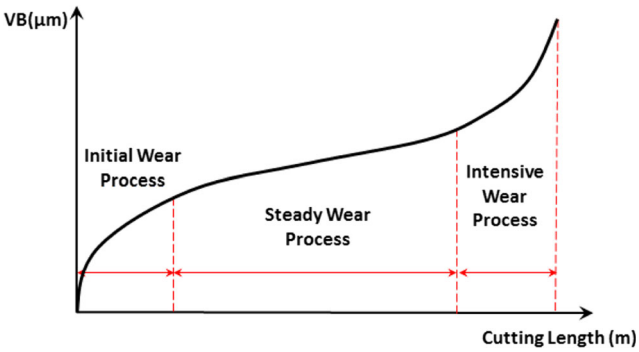

Fig. 1 Three tool wear processes according to the tool life curve

This paper presents the development of an analytical model to investigate the progress and mechanism of flank wear of PCD tools. This is the first time a model was developed by considering the combined effects of tool/workpiece abrasion, adhesion, the dynamic cutting forces, and the properties of different PCD materials. The model was validated by turning titanium alloy Ti6Al4V with three different types of customized PCD tools. Morphology of both worn areas and profile of chips were examined, and in combination with the analysis of dynamic cutting force and simulation results, the wear mechanism of different PCD tools was investigated. The machined surface in micro-scale was further checked to discuss the molecular process between the cutting tool and workpiece in the development of flank wear.

2 Flank wear of PCD tools

It has been proved that the "diffusive-abrasive" interaction at the tool/workpiece interface was the main wear mechanism in machining titanium alloys when using metallic tools [12].

In adhesive wear, a huge amount of heat is generated due to the deformation of the workpiece material. Under the combined effect of normal stress and high temperature, micro-welds [24] are formed between the asperities on both tool flank face and workpiece surface (Fig. 2a). However, for a metal cutting process using PCD tools, no research was ever conducted to investigate the micro-weld process between diamond and metallic material. The adhesion at the tool/workpiece interface was ascribed to the molecular process [25]; specifically, the titanium-carbon joints formed at the interface stimulated by the high environment temperature. Then, the shear of joint could happen on both the tool side and the workpiece side when suffering from external shear stress. Workpiece materials would adhere on the tool surface when the joint shear appears on the workpiece side, while the tool material would be removed if the shear of joint happens on the tool side.

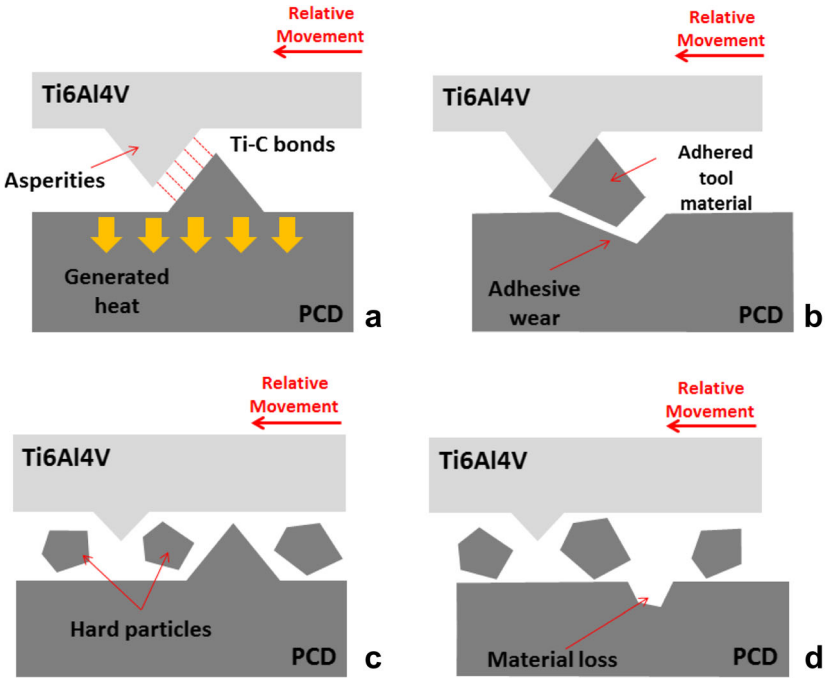

Fig. 2 Simplified mechanism of processes of adhesive wear and abrasive wear. **a** Formation of micro-welds. **b** Material loss due to adhesive wear. **c** Status of three-body abrasion. **d** Material loss due to abrasive wear

Although PCD has ultra-high hardness, the binder material (cobalt in this study) which acts as both the bridge and boundary of the sintered diamond structure could be softened under high temperature. Combined with the tool/workpiece abrasion, the cobalt-diamond bonds could break, and initial cracks could be developed at the cobalt-diamond boundaries, leading to the collapse of the PCD structure [26]. As a result, joint shear is prone to happen on the tool side and causes material loss on the tool flank face (Fig. 2).

Abrasive wear is the facial damage caused by the scratching of either the sliding of hard asperities or the rolling of hard particles at the tool/workpiece interface. The types of abrasion could be classified as two-body mode and three-body mode according to the status of the abrasion. For the two-body abrasion, asperities on the harder side, or strongly constrained hard particles, scratch on the softer side leading to the loss of material on this side. As is for PCD tools, diamond grains or fractured sintered diamond structure could be released in the tool wear processes (Fig. 2). These hard particles roll or slide together with the titanium alloy at the tool/workpiece interface, and could cause further release of hard particles or material loss on the softer surface which is known as three-body abrasion (Fig. 2).

Furthermore, the adhesive-abrasive wear process of PCD is influenced by machining dynamics, mainly the dynamic cutting forces [27]. With the development of tool wear, the cutting edge becomes blunt and the shear of the workpiece material is difficult, which leads to the increase of cutting forces in three directions: feed force (axial direction), back force (radial direction), and main cutting force (tangential direction). Correspondingly, the increase of temperature and pressure at the tool/workpiece interface caused by increasing cutting forces stimulates the adhesive-abrasive wear, which accelerates flank wear directly [28]. As a result, the dynamic cutting forces must be considered when developing the model of the tool wear.

3 Theoretical model

3.1 Tool material loss due to adhesive process

The material loss due to the adhesive process is mainly the removal of Ti-C joints. The amount of adhesive wear per unit area can be calculated with the following equation:

$$W_{unit\_adh} = N \times S_{mw} \times L_{mw} \times P \tag{1}$$

where

W_{unit_adh}	Tool material loss due to the adhesion per unit area (mm^3/mm^2)
N	The number of the Ti-C joints per unit area ($/mm^2$)
P	Probability of forming a certain size of wear fragment; this value can be obtained from the experiments of Rabinowicz [18].
L_{mw}	The length of Ti-C joints (mm)
S_{mw}	The average cross area of each Ti-C joint (mm^2)

According to the results made by Huang et al. [23], the actual contact pressure was a measure of the hardness of the asperities on the softer side. The contact pressure at the cross

section of the micro-welds, P_{ac}, is equal to the hardness of the workpiece material, which could be calculated as follows:

$$P_{ac} = \frac{F_n^m}{S_{mw} \times N \times S_{fw}} = \frac{F_n^m}{S_{mw} \times N \times a_p \times VB} = H_w \quad (2)$$

where

F_n Normal force exerted on the flank face (N)
S_{fw} Total contact area on the worn tool flank face, which equals to the product of width of flank wear and the cutting depth (mm^2)
a_p Depth of cut (mm)
VB Width of flank wear, maximum in this study (mm)
H_w Hardness of the softer material (MPa)
m Adhesive constant depending on the type of deformation during the wear process (Table 1)

The volume of material loss per unit area caused by adhesive process is expressed as

$$W_{unit\_adh} = NS_{mw}L_{mw}P = \frac{F_n^m \times N \times P \times L_{mw}}{H_w \times N \times a_p \times VB} = \frac{F_n^m P L_{mw}}{H_w a_p VB} \quad (3)$$

where the average cross-section area of each micro-weld is

$$S_{mw} = \frac{F_n^m}{H_w \times N \times a_p \times VB} \quad (4)$$

Considering that the tool/workpiece contact area in time dt is the sliding area during this period of machining time, as a result, the rate of material loss caused by adhesive process in dt is expressed as

$$\frac{dW_{adh}}{dt} = \frac{ds \times \left(a_p \times W_{uint\_adh}\right)}{dt} = V_c a_p W_{unit\_adh} = \frac{F_n^m V_c P h_{mw}}{H_w VB} \quad (5)$$

Table 1 Adhesive constant [29]

Deformation type	Shape of adhesion	m
Elastic	Layer	0.6
	Lump	0.8
Plastic	Layer	0.75
	Lump	1

where

W_{adh} Tool material loss due to the adhesion (mm^3)
s Sliding distance (mm)
V_c Cutting speed (mm/min)
dt Time period (s)

3.2 Tool material loss due to abrasion process

Based on the empirical-quantitative model proposed by Rabinowicz et al. [18], the volume of material loss caused by three-body abrasion can be calculated with the following equation:

$$W_{abr} = \frac{s \times F_n \times \tan\theta}{K} \times \frac{H_w^{n-1}}{H_t^n} \quad (6)$$

where

W_{abr} Tool material loss due to the three-body abrasion (mm^3)
K Constant depending on the type of abrasion
s Sliding distance (m)
H_w Hardness of the workpiece (MPa)
H_t Hardness of the cutting tool (MPa)
n Constants depending on the ratio of tool/workpiece hardness
F_n Normal force exerted on the flank face (N)
θ Surface contact angle in the abrasive process, which is 45° in this study

Parameters K and n were selected based on the ratio of tool hardness and workpiece hardness (Table 2). To consider the rate of tool material loss due to abrasive wear, the equation was differentiated on both sides w.r.t. time; as a result, the rate of material loss caused by the adhesive process in dt is expressed as

$$\frac{dW_{adr}}{dt} = \frac{ds}{dt} \times \frac{F_n \times tan\theta}{K} \times \frac{H_w^{n-1}}{H_t^n} = \frac{V_c \times F_n}{2.43} \times \frac{H_w^6}{H_t^7} \quad (7)$$

Table 2 The constants K and n [18]

Hardness ratio	K	n
$H_t/H_w \le 0.8$	3	1
$0.8 \le H_t/H_w \le 1.25$	5.3	3.5
$H_t/H_w \ge 1.25$	2.43	7

3.3 Normal force

Since the normal force is changing in accordance with the development of flank wear, it is critical to develop an accurate model to calculate the normal force in each cutting period. When the cutting edge is sharp, the force exerted normal to the cutting edge can be calculated according to the classical shearing and ploughing model [30]

$$F_{ns} = K_{ns}A + K_{np}L_{edge} \tag{8}$$

In this model, A and L_{edge} are the area undeformed chip section and the length of engaged cutting edge, respectively. The constant K_{ns} is the shearing constant describing the effect of normal rake on the normal force, and K_{np} is the ploughing constant due to clearance friction on the machined surface. Both constants can be determined by using the method developed by Wang et al. [31].

With the development of flank wear, the force normal to the worn flank surface could be regarded as the sum of the normal force exerted on the blunt cutting edge which was considered to be the same value as F_{ns}, and the component force exerted the flank wear area, F_{nw} (Fig. 3b). The force exerted on the flank wear area, F_{nw}, is calculated by the product of the normal stress σ_w and the flank wear area S_w:

$$F_{nw} = S_w\sigma_w = a_p{\cdot}VB{\cdot}\sigma_w \tag{9}$$

To estimate stress σ_w exerted on the worn surface, the fracture of PCD has to be taken into account. Because tool material loss in wear process is caused by the fracture of PCD structure when it suffers from external stress, the relationship among exerted stress σ, fracture distance r, and fracture toughness K_{Ic} can be described as follows [32]:

$$\sigma = \frac{K_{Ic}}{\sqrt{2\pi r}} \tag{10}$$

The geometric relationship between fracture distance r and increment of flank wear width is shown in Fig. 4. Parameter r is defined to be equal to the thickness of the removed tool material layer $(r_2 - r_1)$ in the wear process of the time period dt. According to the geometric relationship, r_1 and r_2 can be calculated as

$$r_1 = (VB_1 - r_1{\cdot}\tan\gamma) \times \tan\alpha \tag{11}$$

$$r_2 = (VB_2 - r_2{\cdot}\tan\gamma) \times \tan\alpha \tag{12}$$

where

dVB	Increment of flank wear landing in time interval dt;
VB_1	Flank wear landing before cutting;
VB_2	Flank wear landing after the time interval dt (current VB)
α	Tool clearance angle
γ	Tool rake angle

3.4 Wear model

According to the geometric relationship shown in Fig. 4, the volume of material loss dV caused by flank wear after dt can be described with the following equation:

$$\begin{aligned} dV &= a_p \times \frac{1}{2} \times (VB_1 + VB_2) \times (r_2 - r_1) \\ &= a_p \times \frac{1}{2} \times (2VB_2 - dVB) \times r \end{aligned} \tag{13}$$

When time interval dt was extremely short, both dVB and r were small and their product was considered as zero. Combined with Eqs. 11 and 12, the increment of wear amount during the time period dt could be written as

$$dV \approx a_p \times VB \times r = \frac{a_p \times dVB \times VB \times \tan\gamma}{1 + \tan\alpha \times \tan\gamma} \tag{14}$$

The total volume of material loss due to the adhesive-abrasive wear process which consists of adhesion and three-body abrasion during the time interval could be expressed as

$$dV = dW_{adh} + dW_{abr} \tag{15}$$

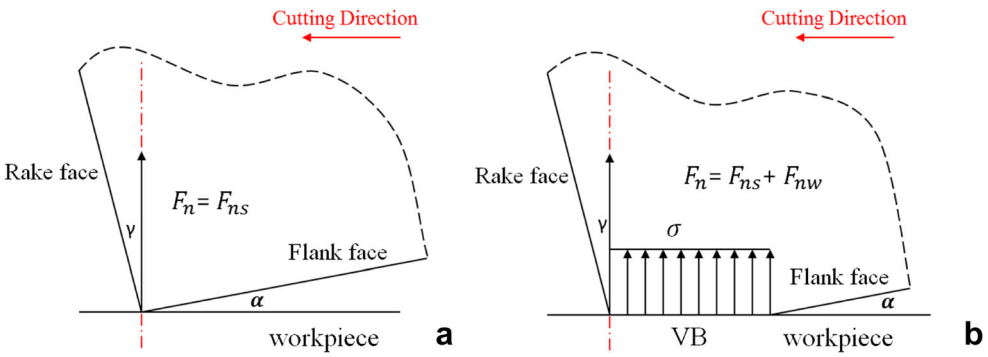

Fig. 3 Cutting force normal to the workpiece interface. **a** Normal force when the tool is sharp. **b** Normal force on the worn flank face

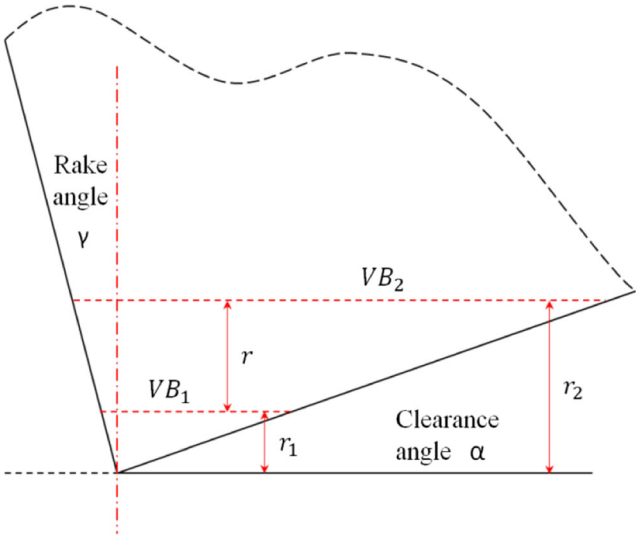

Fig. 4 Geometric relationship between VB and wear volume

Differentiating both sides w.r.t. time, the above equation (Eq. 15) could be re-written as follows:

$$\frac{dV}{dt} = \frac{dW_{adh}}{dt} + \frac{dW_{abr}}{dt} = \frac{C_1}{VB} + \frac{C_2}{VB^2} \tag{16}$$

where

$$C_1 = \frac{(1-\omega) F_n V_c H_w^6}{2.43 H_t^7 a_p \left(\frac{\tan\gamma}{1 + \tan\alpha \times \tan\gamma} \right)}$$

$$C_2 = \frac{\omega F_n^m V_c P h_{mw}}{H_w a_p \left(\frac{\tan\gamma}{1 + \tan\alpha \times \tan\gamma} \right)}.$$

where

ω A parameter to describe the proportion of normal force exerted on the sum area of the micro-welds cross section. In this study, the value was adopted as 0.5.

The calculation was conducted by using MatLab2016R. The flow chart of the calculation is shown in Fig. 5. Initially, the cutting force of sharp tools was calculated by using the pre-set cutting parameters. Using the properties of PCD material listed in Table 3 and the properties of workpiece Ti6Al4V in Table 5, the amounts of material loss caused by both adhesive wear and abrasive wear were calculated and the differential equation describing the relationship between the flank wear rate and wear volume was developed. The flank wear in the fixed time interval could be obtained by solving the differential equation, and this value was used to calculate the normal force in the next time interval.

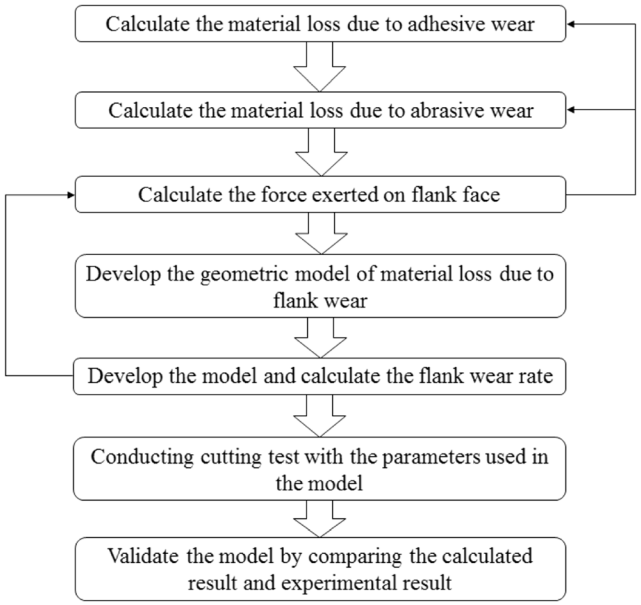

Fig. 5 Calculation process of the model of flank wear

4 Experiment

Since the model was developed based on orthogonal cutting, a series of turning tests were conducted to validate the model and its capability.

4.1 Preparation of cutting tools

Three types of PCD materials, CTB002 (Fig. 6a), CTB010 (Fig. 6b), and CTM302 (Fig. 6c), manufactured by Element Six were used as the tool materials. As listed in Table 3, the sizes of diamond grains of CTB002, CTB010, and CTM302 are 2 μm, 10 μm, and the mix of 2 to 30 μm, respectively. The volume percentage of diamond of CTM302 is 91.4%, which is bigger than that of CTB010 (around 89%) and CTB002 (around 85%). The tool inserts were firstly cut from a PCD disc into cubic shapes (7 mm × 7 mm) by wire-cut EDM (W-EDM). After W-EDM machining, graphitization and tensile residual stress existed within a certain depth under the machined surface because of the thermal defects caused by the EDM plasma. In order to remove the defects in the "heat-affected zone" (HAZ), flank faces of the inserts were refined by conventional abrasive grinding, which was conducted on a CNC diamond grinder Coborn RG6-FE. The machining in-feed for abrasive grinding was around 100 μm to ensure the HAZ was removed. Parameters of abrasive grinding (feed rate of 0.2 mm/min and cutting speed of 10 m/s) were optimized to avoid significant compressive residual stress in the grinding process. The radius of the cutting edge and the roughness of machined surfaces are listed in Table 4.

Table 3 Basic physical properties of PCD materials [33]

Workpiece material	CTB002	CTB010	CTM302
PCD layer thickness (mm)	0.5	0.5	0.5
Diamond fraction (vol %)	84.8%	89.7%	91.4%
Grain size (μm)	2	10	2 to 30
Hardness (MPa)	5000	5000	5000
Young's modulus (GPa)	901	1000	883
Bending strength (MPa)	1999	1741	1131
Fracture toughness (MPa m-1/2)	8.05	8.96	8.34
Thermal conductivity (W m^{-1} K^{-1})	239	456	422

4.2 Selection of workpiece material

The workpiece used in this study was Ti alloy robs made of Ti-6Al-4V grade 5 with the dimension of 300 mm in length and 50 mm in diameter. The attractive physical properties (Table 5), outstanding resistance to chemical erosion, and inherent workability make Ti6Al4V most widely used titanium alloy in industry. However, the strong affinity of titanium with oxygen increases with temperature and the surface oxide layer increases in thickness at elevated temperatures. Under the temperature over 800 K, the metal becomes highly susceptible to embrittlement by oxygen, nitrogen, and hydrogen, which dissolve interstitially in titanium [34]. As a result, the cutting experiment was conducted under an 8-MPa coolant (Rocol Ultracut Clear) to avoid the thermal damages on both cutting tools and machined surfaces.

4.3 Experimental setup and data processing

The turning experiment was conducted on a CNC lathe OKUMA GENOS L200E-M (Fig. 7a). Since tool inserts were shaped into cuboids, the tool geometric parameters were determined by the tool holder: rake angle − 10°, clearance angle 10°, and cutting edge angle 45° (Fig. 7b). The tips of three tools were sharped with both corner radius and cutting edge radius being around 5 μm. A specially designed tool fixture was fabricated with aluminum alloy for the measurement of cutting force by clamping the tool holder and dynamometer (PCB Piezotronics 260A01) together as a rigid body (Fig. 7c).

Table 4 Sharpness and roughness after grinding

Material	CTB002	CTB010	CTM302
Sharpness (μm)	5.42	5.92	6.48
Roughness (nm)	111	121	129

The PCD insert was fastened on the tool holder, and the dynamometer was mounted on the base of the tool holder. The entire experiment was divided into three groups, and the workpiece was machined with one type of PCD insert in each group. Each cutting test consists of 14 turning processes, each of which lasted 50 s. Same cutting parameters which were practically used in finishing processes with PCD tools in industry [35] were applied in all experiments: cutting speed 160 m/min, feed rate 0.15 mm/rev, and cutting depth 0.2 mm. Cutting forces exerted on the PCD tool were measured by a dynamometer (Kistler 5070A) in three directions: feed force (axial direction), back force (radial direction), and main cutting force (tangential direction). For each cutting process, force signals were firstly acquired by the dynamometer as analog signal and amplified by the coupler (Kistler 9527B); a DAQ card (National Instruments 6036E) was used to condition the signal and complete the A/D conversion, and LabVIEW SignalExpress was used to process the signal. The acquired cutting force signals were filtered with MatLab using Chebyshev filtering program to remove noises. The filtered voltage data was converted into force by multiplying the sensitivities of the dynamometer in each direction.

4.4 Flank wear measurement

After each cutting pass, flank wear, nose wear, and crater wear were examined by an Alicona optical microscope. Values of maximum flank wear which are defined as VBs (Fig. 8) were plotted to reflect the development of tool wear. Tools would be rejected if they satisfied one of the following tool failure criteria (ISO 3685-1993): maximum flank wear reached 0.4 mm or any catastrophic fracture appeared on the cutting edge. The cutting experiment was repeated twice to ensure reliability of the experimental data, and the VBs after each

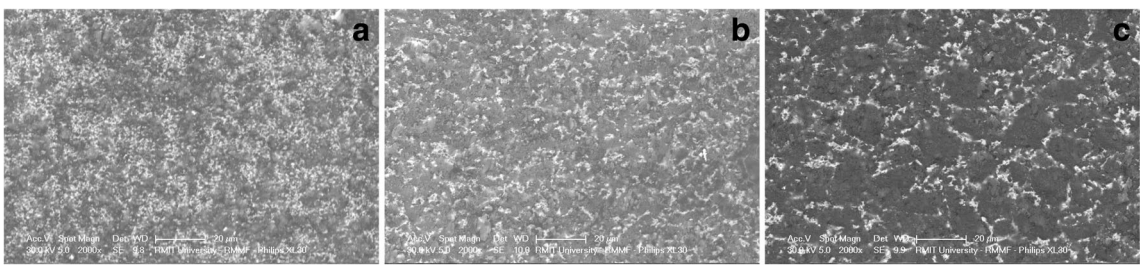

Fig. 6 Three types of PCD materials. **a** CTB002. **b** CTB010. **c** CTM302

Table 5 Basic physical properties of Ti-6Al-4V

Material	Density	Hardness (HV)	Elastic modulus	Poisson's ratio	Thermal conductivity
Ti-6Al-4V	4.43 g/mm^3	349 Kgf/mm^2	113.8 GPa	0.342	6.7 W/m.K

cutting passes were measured three times to reduce the error caused by the measurement.

5 Model validation and discussion

5.1 Model validation

The results calculated with the proposed model and the VBs measured in the cutting experiments are plotted in Fig. 9 to show the development of flank wear. It can be seen that the measured VBs of all three tools increased steadily in a linear trend, and the development of tool wear caused by the abrasive process was steeper than the increase of flank wear caused by the adhesive process. The VBs were measured after each 50-s cutting process and plotted with the same time interval (cutting process). The largest VBs were found when the tool CTB002 was used (186 μm), followed by the VBs of CTB010 tool (133 μm). The tool made of CTM302 showed the best resistance to flank wear because of the lowest VB after 14 cutting passes (124 μm). The measured VBs increased linearly; this trend matches the trend of calculated results when tools CTB002 and CTB010 were used. As for the tool CTM302, sudden increments of VB were found after the 1st, the 9th, and the 14th cutting passes, respectively. The increments of VBs in the 5th to the 8th cutting passes and the 10th to the 13th cutting passes were insignificant. To validate the model and to investigate the wear process of the three different types of tools, a comparison between the calculated values and experimental results was presented by the percentage deviation which was calculated with the following equation:

$$\text{Deviation} = \left| \frac{VB_{measured} - VB_{calculated}}{VB_{measured}} \right| \times 100\% \quad (17)$$

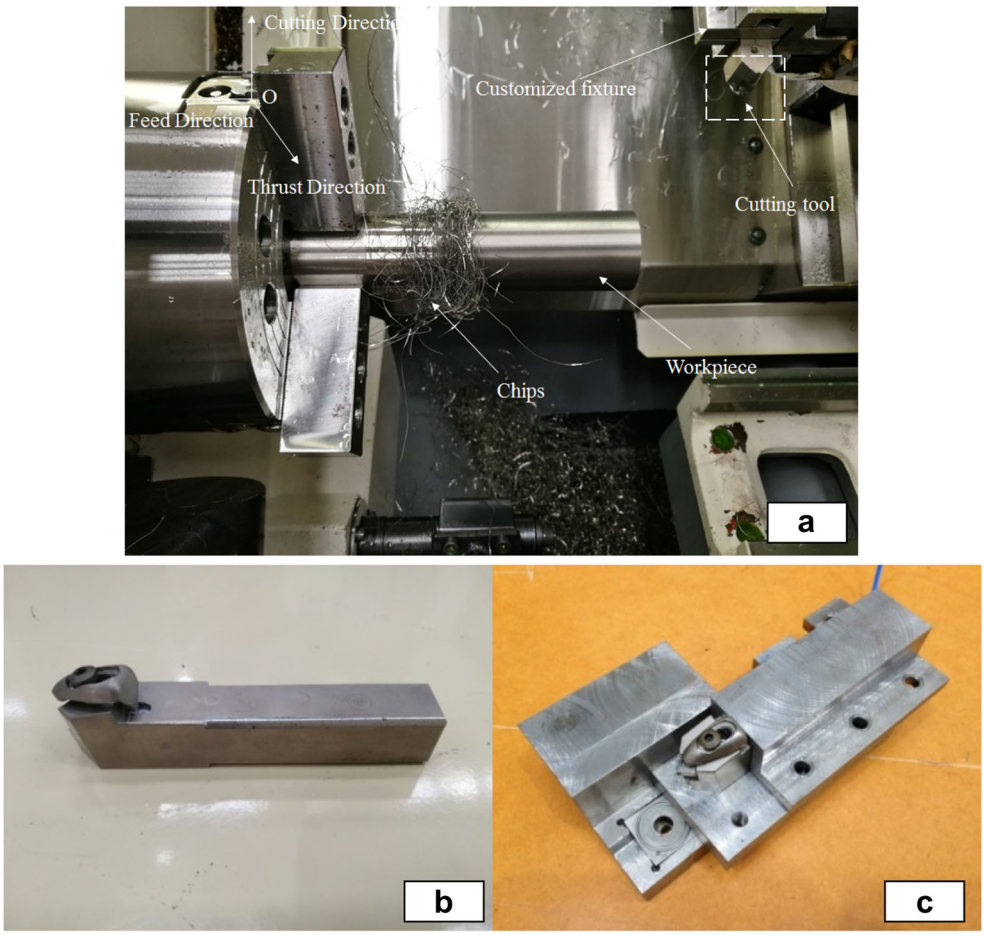

Fig. 7 **a** Experimental setup of the turning tests. **b** Tool holder. **c** Designed tool holder

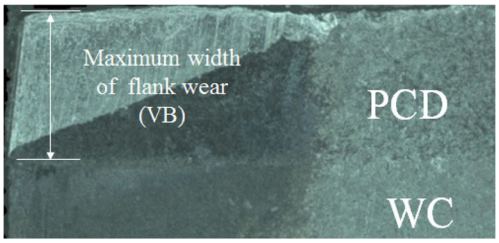

Fig. 8 Measurement of flank wear (VB)

According to the results of calculation, the deviations of CTB002, CTB010, and CTM302 are generally below 10% except for a few abnormal results which are caused by special reasons explained in Sect. 5.2. The experimental results of tool CTB010 distributed along the linearly calculated results indicating that the development of flank wear was dominated by the adhesive-abrasive process. The measured VBs were larger than the calculated results considering adhesive-abrasive wear when the tool CTB002 was used, indicating that the adhesive wear contributed more in the material loss process of flank wear. In contrast, the deviations of tool CTM302 was bigger and the fluctuation irregularly. This abnormal difference was caused by the large-scale fracture which is discussed in Sect. 5.2.

The cutting forces in the three directions increased with the increase of cutting passes. When tools made of CTB002 and CTB010 were used, the main cutting forces increased from around 100 N to over 400 N with a near-linear trend (Fig. 10a). Different from CTB010 and CTB002, sudden increases of main cutting force in some cutting passes were found when the CTM302 tool was used. The trends of feed force (Fig. 10b) are similar to that of tangential force. The cutting force increased linearly when tools CTB002 and CTB010 were used, while the force experienced sudden increases when the tool CTM302 was used. The thrust force increased linearly for all three tools (Fig. 10c), the forces of CTB002 and CTB010 increased with a steeper gradient from the 1st to the 8th cutting and it experienced insignificant increase afterwards. In contrast, the radial force of CTM302 had a different trend, and the increment was insignificant in the first nine cutting passes, while there was a sudden increase in the 10th cutting process and it became stable again afterwards.

5.2 Discussion

From the development of VBs and cutting forces, it was found that the wear mechanisms of the tools made of three PCD

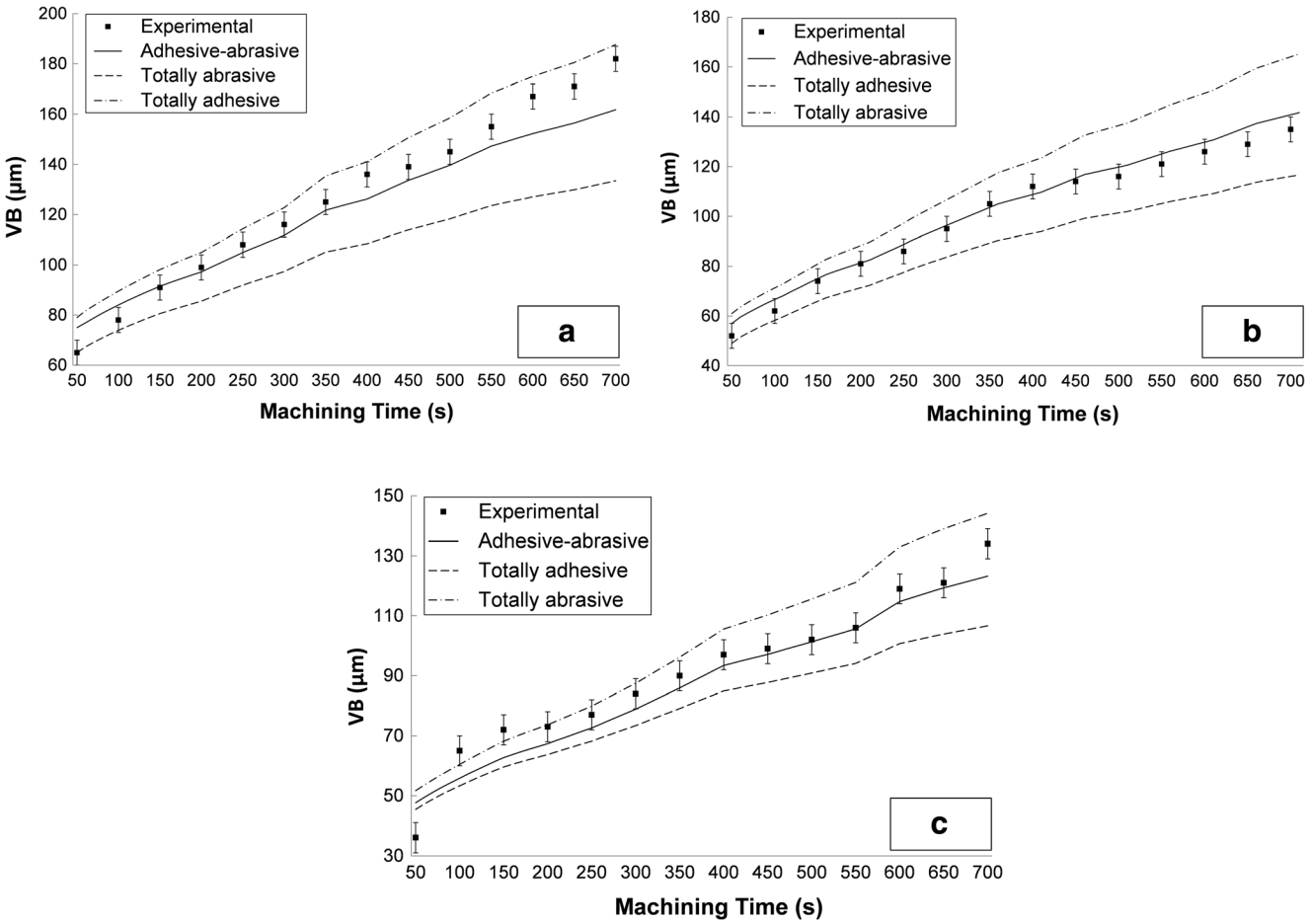

Fig. 9 Experimental and calculated results of width of flank wear. **a** Tool CTB002. **b** Tool CTB010. **c** Tool CTM302

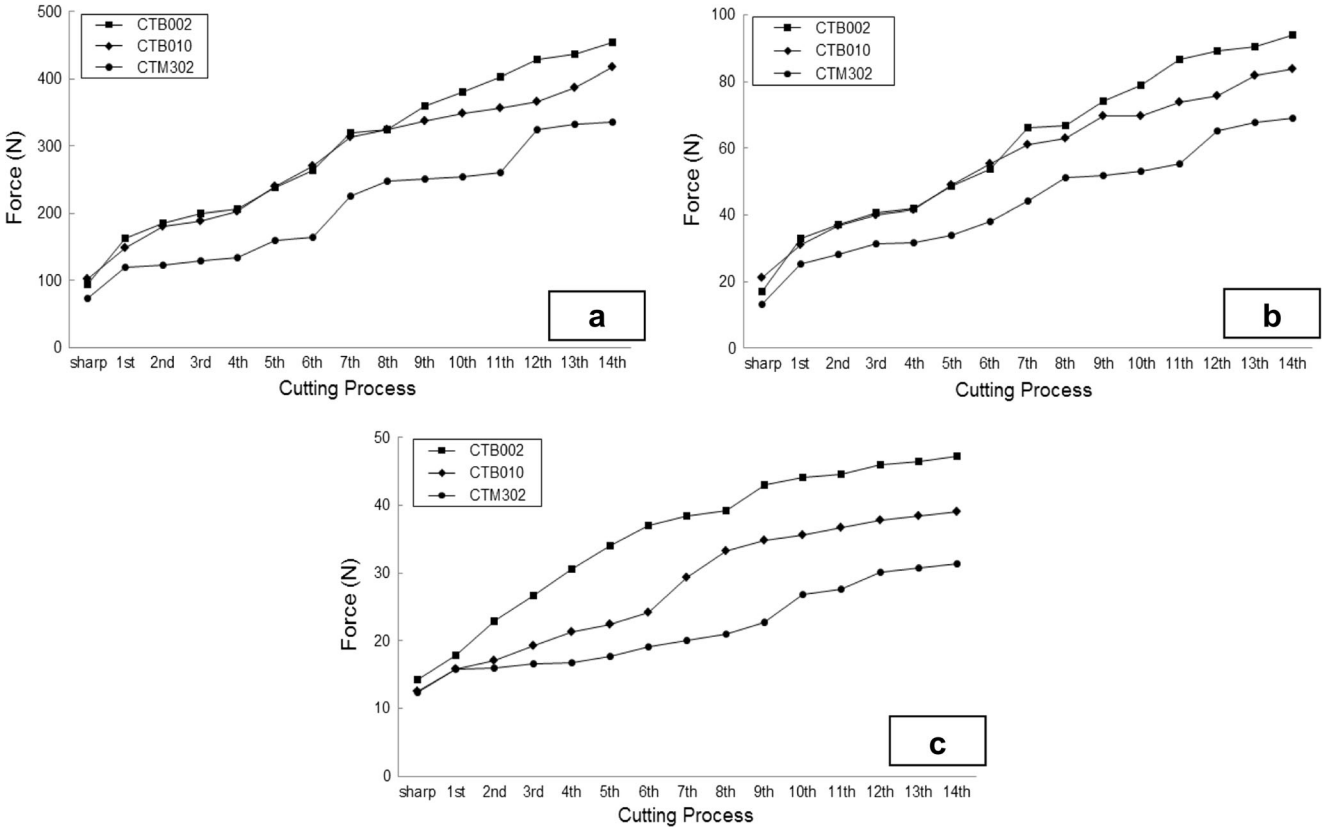

Fig. 10 Cutting forces in different directions. **a** Main cutting force (tangential direction). **b** Feed force (axial direction). **c** Thrust force (radial direction)

materials were different. To investigate the wear mechanism, morphological characters of the worn area on the flank face of each tool were examined by using Philips XL30 Scanning Electron Microscope (SEM). As shown in Fig. 11a, b, worn areas near the tips of tools CTB002 and CTB010 were relatively flat, scaled with partial workpiece material after six cutting passes. The boundary between the exposed area and the adhesion-rich area on the flank face of tool CTB002 and the scratches adhered on the worn surface of tool CTB010 demonstrated that a layer of adhesion was ever formed, but it was partially removed together with some tool materials in the cutting process. This was similar to the worn morphology found in the cutting test conducted by Li et al. [36]. As for the morphology of flank wear after the following eight cutting passes, a huge amount of titanium alloy stacked on the tool nose, and the thickness of adhesion layers was bigger than those formed after six cutting passes were conducted (Fig. 11, d).

As was proved in the sliding tests and milling processes [10, 37], because of the breakage of diamond-to-diamond bonds and diamond-to-cobalt bonds, cracks could develop at the interface of bonded diamond grains and cobalt-diamond interfaces (intergranular fracture) of the polycrystalline diamond structure (Fig. 12a). With the development of cracks, the tool material with adhered workpiece material was prone to being removed by the tool/workpiece abrasion as a "spalling" process [8]. In this study, PCD materials on the flank faces of tools CTB002 and CTB010 were removed "layer by layer" as the cycle of formation and abrasion of adhesion layer during the flank wear process. Due to the poor cooling effect, this spalling process was more severe at the tool/workpiece interface near the tool tips. During the cutting processes, the heat caused by the deformation of the workpiece material was increased due to the increase of cutting force which caused the bluntness of cutting edges. Combined with the low thermal conductivity of titanium alloy, temperature near the tips of the tools increased drastically, stimulating the adhesion of titanium alloy at the tool tips. Compared with CTB002, the thermal conductivity and fracture toughness of CTB010 are better due to the higher volume percentage of diamond and larger diamond grains. This made the tool made of CTB010 more resistant to the "spalling" wear process on flank face.

In contrast, the wear mechanism of tool CTM302 was different from the tools made of CTB002 and CTB010. Different from the PCD materials which consist of even-size grains, CTM302 was manufactured with both small-size and large-size diamond grains (2 to 30 μm). Due to higher volume fraction of diamond and larger diamond grains, the tools made of this PCD material are more resistant to tool/workpiece abrasion but more fragile. Based on the results of McNamara et al., trans-granular fracture (Fig. 12b) could happen at the cleavage plane in large-size diamond grains when the PCD consisted of

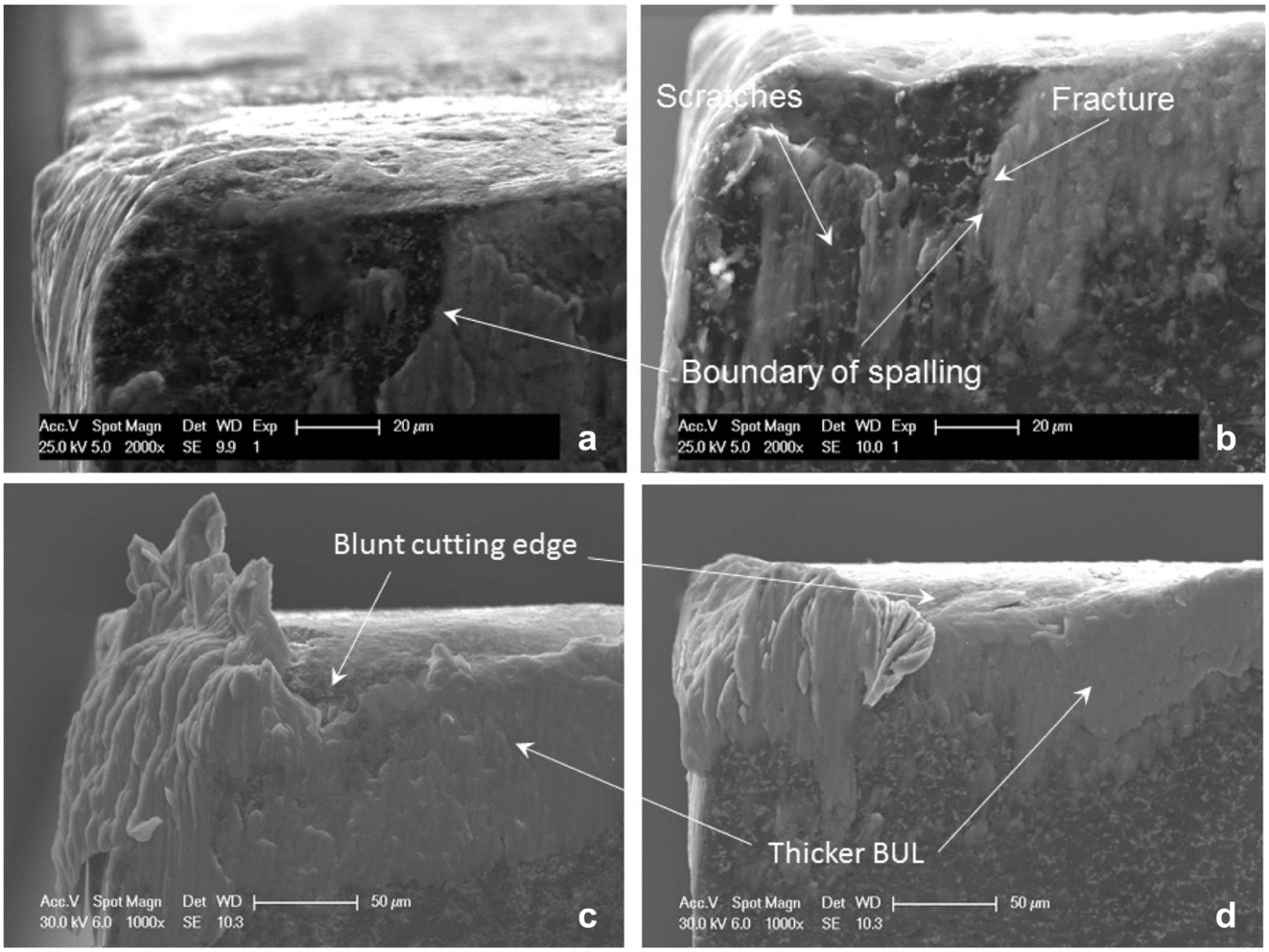

Fig. 11 Wear mechanism of PCD tools. **a** The tool CTB002 after six cutting passes. **b** The tool CTB010 after six cutting passes. **c** The tool CTB002 after 14 cutting passes. **d** The tool CTB010 after 14 cutting passes

30 μm diamond grains [38]. With the development of inter-granular fracture and trans-granular fracture, large-scale collapse of PCD might happen when the tool CTM302 was used. Instead of the steady spalling process, tool materials were lost due to the fracture of the tool tip in the cutting process in the first three cutting passes. This large-scale fracture led to a significant increase in VB, which explained the significant deviation between the calculated and experimental results.

Also, the morphological characters of the worn surface proved that the large-scale fracture kept happening at the tip of tool CTM302. The SEM image obtained after six cutting passes shows (Fig. 13a) that the tip was significantly removed

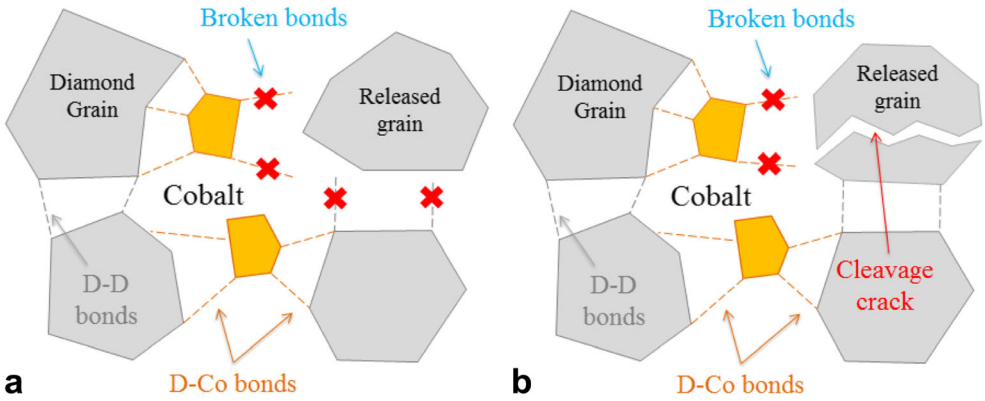

Fig. 12 Fracture of PCD structure in micro-scale. **a** Inter-granular fracture. **b** Trans-granular fracture

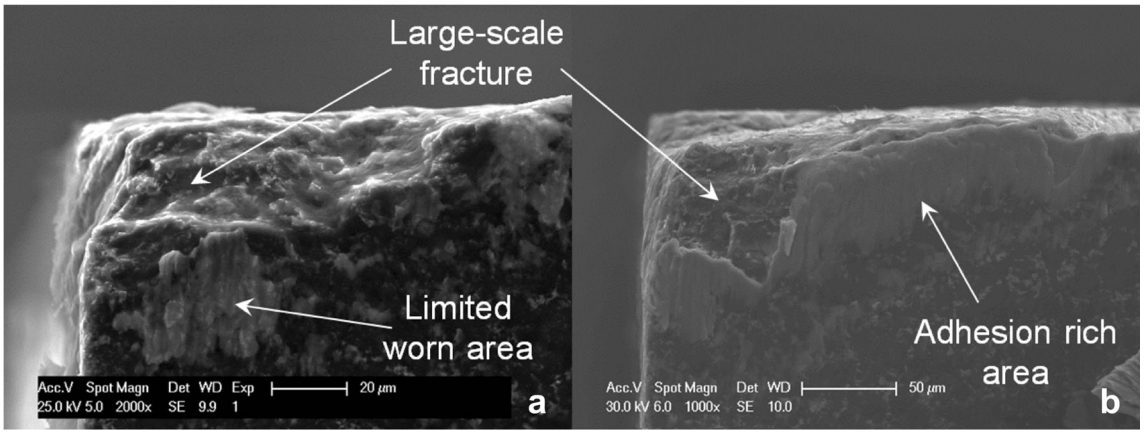

Fig. 13 **a** Worn area of tool CTM302 after six cutting passes. **b** Worn area of tool CTM302 after 14 cutting passes

by large-scale fracture, leaving a coarse surface at the position when the tool made of CTM302 was used. It can be seen that the area of adhesion layer was limited on the flank face. Large-scale fracture kept happening during the following eight cutting passes (Fig. 13b). The fracture area near the tool tip was larger without any workpiece material scaled on. Also, the thick layer of titanium which adhered to the tool at the boundary of fracture indicated that the tool/workpiece contact area increased before the fracture of the tool tip.

To further investigate the wear process of tool CTM302, the difference in chip curvature chips which indicated the changing of tool/chip contact length [39] was analyzed. As can be seen in Fig. 14, helical chips were generated in the first cutting test when the tool tip was intact. In the following five cutting passes, the shape of the chip changed from short-curled to discontinuous because of the fracture of the tool nose during the cutting process. Specifically, a coarse worn surface with a larger rake angle was formed due to the fracture, and this concave area played the role of a chip breaker stimulating the formation of discontinuous chips. With the continuation of the cutting, a coarse concave surface was flattened by the tool/chip abrasion, which eliminated the chip breaker caused by the breakage of the tool tip (Fig. 15b). This increased the tool/chip contact length, and long-curled continuous chips were prone to being generated from the 7th to the 9th cutting passes. The fragment chips generated in the last three cutting passes clearly indicated the appearance of the tool tip fracture (Fig. 15c).

Machined surfaces were examined after 14 cutting passes in micro-scale (Fig. 16), and wavy profiles were found on the surfaces due to the profile of the tool nose. As was found in the images with larger magnification, there were no obvious flaws such as fracture or scratches on the machined surface. Also, the irregular deformation of the peak of the wavy profile indicated that the temperature was extremely high during the cutting. The aforementioned molecular process [25] between

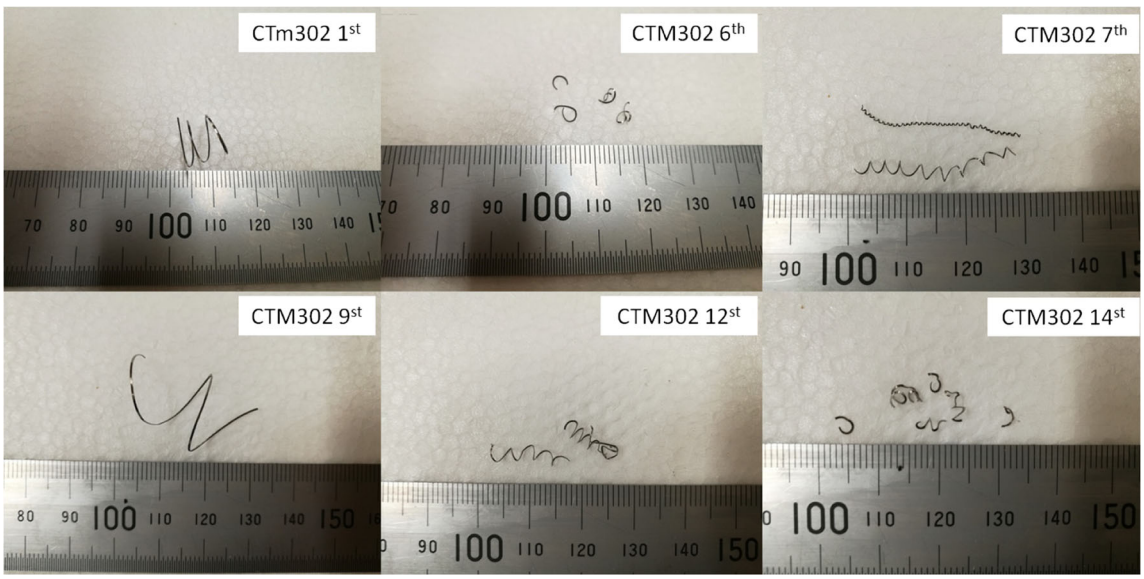

Fig. 14 Chip morphology after different cutting passes using the tool CTM302

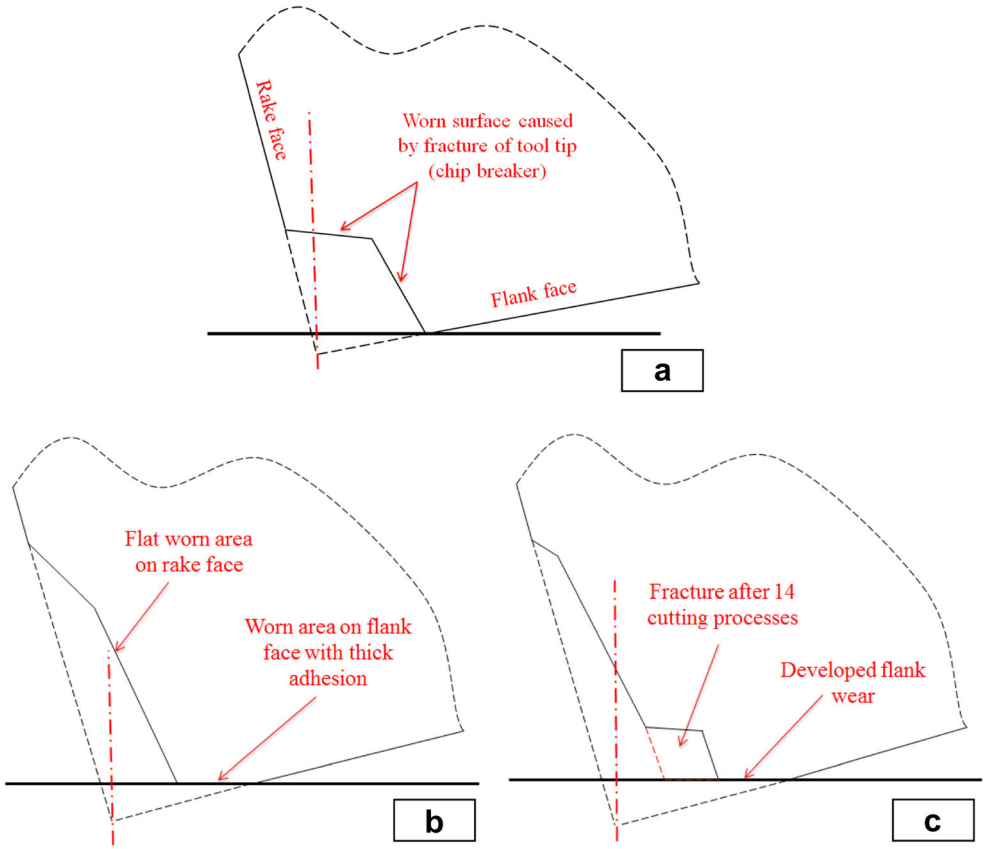

Fig. 15 Simplified wear process of PCD tools. **a** Fracture of tool tip after six cutting passes. **b** The change of tool geometry due to the fracture of tool tip. **c** Fracture of the tool tip after 14 cutting passes

the titanium alloy and PCD were proved by the results of energy-dispersive X-ray spectroscopy (Fig. 17). The existence of carbon proved that the carbon diffused into the machined surface in the molecular process due to the tool/workpiece abrasion, and it was found that the atom percentage of the carbon was different for the surfaces machined by different PCD tools. Higher percentages were found on the surface machined by tools CTB002 and CTB010. This proved that the temperatures during the cutting processes were higher, and the molecules between the tool material and workpiece material were intensive. In comparison, the lower atom percentage of carbon found on the surface machined by tool CTM302

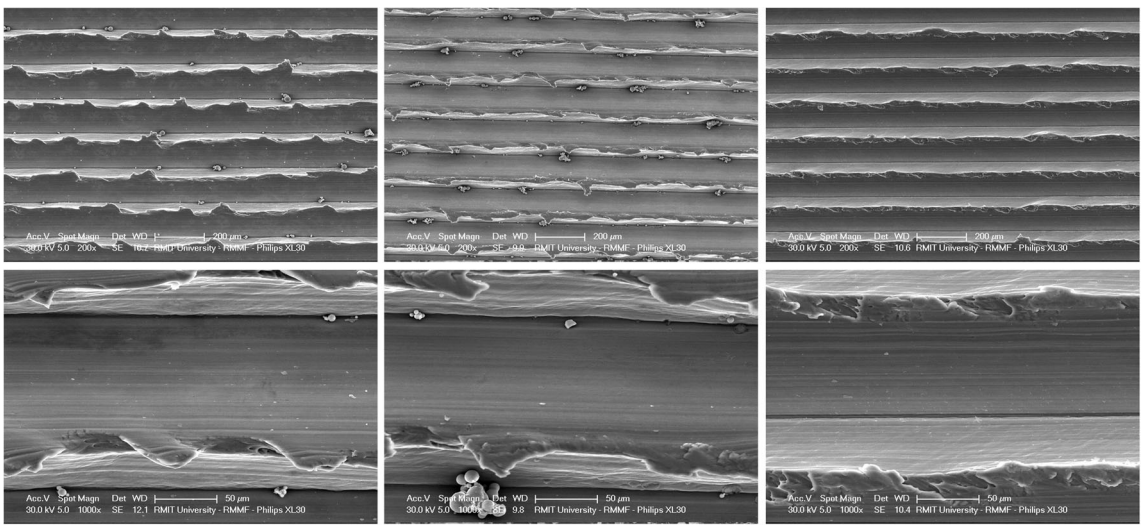

Fig. 16 Morphology of surfaces machined by different PCD tools in micro-scale

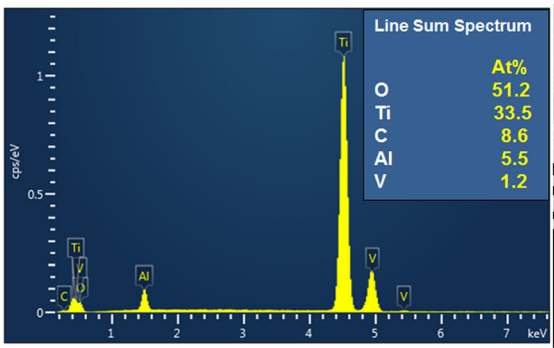

Cutting Tool	Carbon %
CTB002	13
CTB010	8.6
CTM302	4.9

Fig. 17 Results of EDS analysis (lines-can) on the machined surface

indicates that the temperature increase caused by the fracture of tool tip was less significant.

6 Conclusion

An analytical model was developed to investigate the wear mechanism of PCD tools in metallic cutting processes. The development of flank wear was calculated by taking into account tool geometry, cutting parameters, and physical properties of workpiece and PCD materials. The model was developed based on the combined influences of adhesive-abrasive process and the dynamic cutting forces, and was validated by turning titanium alloy Ti6Al4V with customized tools made of three PCD materials. The comparison between the calculated results and experimental data showed that the VBs calculated with the proposed model match the actual values when tools CTB002 and CTB010 were used. With the development of flank wear, the effect of abrasive wear became more significant on the tool made of CTB002. The wear mechanism of the tool made of CTM302 was different, and this led to obvious deviation between the experimental and calculated results in some cutting passes.

By analyzing the morphological characters of worn areas as well as the chips, it was found that in tools made of CTB002 and CTB010 worn in a steady "spalling" process, the PCD material was removed layer by layer during the cycle of formation and removal of adhesion layers. This was in accordance with the linearly increased cutting forces in tangential direction. Large-scale fracture happened in the cutting tests when adopting tool CTM302, and the influence on the tool profile, which changed the tool/workpiece contact area, resulted in the change of chip shapes between continuous and discontinuous throughout the experiment. The examination of the machined surface in micro-scale showed that no catastrophic damage was found, and the result of EDS showed that the molecular process between the three tools and workpiece materials were different.

References

1. Kuljanic E, Fioretti M, Beltrame L, Miani F (1998) Milling titanium compressor blades with PCD cutter. CIRP Ann Manuf Technol 47(1):61–64
2. Liang L, Liu X, Li X, Li Y (2015) Wear mechanisms of WC–10Ni3Al carbide tool in dry turning of Ti6Al4V. Int J Refract Met Hard Mater 48(0):272–285
3. Ding S, Yuan R, Li Z, Wang K (2006) CNC electrical discharge rough machining of turbine blades. Proceedings of the Institution of Mechanical Engineers. Part B: J Eng Manuf 220(7):1027–1034
4. Ding S, Yang D, Han Z (2005) Boundary-conformed machining of turbine blades, Proceedings of the Institution of Mechanical Engineers. Part B: J Eng Manuf 219(3):255–263
5. Liu Q, Mahdavian S, Aswin D, Ding S (2009) Experimental study of temperature and clamping force during Nd:YAG laser butt welding. Opt Laser Technol 41(6):794–799
6. Blank V, Popov M, Piovarov G, Lvova N, Gogolinsky K, Reshetov V (1998) Ultrahard and superhard phases of fullerite C60: comparison with diamond on hardness and wear. Diam Relat Mater 7(2–5): 427–431
7. Pan W, Karmaruddin A, Ding S, Mo J (2014) Experimental investigation of end milling of titanium alloys with polycrystalline diamond tools. Proc Inst Mech Eng B J Eng Manuf 228(8):832–844
8. G. Oosthuizen, G. Akdogan and N. Treurnicht, The performance of PCD tools in high-speed milling of Ti6Al4V. Int J Adv Manuf Technol, 2011. 52(9–12): p. 929–935.
9. Stephenson D and Agapiou J (2005) Metal cutting theory and practice. Vol. 68: CRC press.
10. Amin A, Ismail A, Khairusshima M (2007) Effectiveness of uncoated WC–Co and PCD inserts in end milling of titanium alloy—Ti–6Al–4V. J Mater Process Technol 192:147–158
11. Li A, Zhao J, Wang D, Zhao J, Dong Y (2013) Failure mechanisms of a PCD tool in high-speed face milling of Ti–6Al–4 V alloy. Int J Adv Manuf Technol 67(9–12):1959–1966
12. da Silva RB et al (2013) Tool life and wear mechanisms in high speed machining of Ti–6Al–4 V alloy with PCD tools under various coolant pressures. J Mater Process Technol 213(8):1459–1464
13. Kannatey-Asibu J (1985) A Transport-diffusion equation in metal cutting and its application to analysis of the rate of flank wear. J Eng Ind 107(1):81–89
14. Hartung P, Kramer B, Von Turkovich B (1982) Tool wear in titanium machining. CIRP Ann-Manuf Technol 31(1):75–80
15. Kronenberg M (1970) Replacing the Taylor formula by a new tool life equation. Int J Mach Tool Des Res 10(2):193–202
16. Takeyama H, Murata R (1963) Basic investigation of tool wear. J Manuf Sci Eng 85(1):33–37
17. Smithey DW, Kapoor SG, DeVor RE (2000) A worn tool force model for three-dimensional cutting operations. Int J Mach Tools Manuf 40(13):1929–1950

18. Rabinowicz E, Dunn L, Russell P (1961) A study of abrasive wear under three-body conditions. Wear 4(5):345–355
19. Bhattacharyya A, Ham I (1969) Analysis of tool wear—part I: theoretical models of flank wear. J Eng Ind 91(3):790–796
20. Choudhury S, Srinivas P (2004) Tool wear prediction in turning. J Mater Process Technol 153–154:276–280
21. Wong T, Kim W, Kwon P (2004) Experimental support for a model-based prediction of tool wear. Wear 257(7–8):790–798
22. Dawson T, Kurfess T (2004) Modeling the progression of flank wear on uncoated and ceramic-coated polycrystalline cubic boron nitride tools in hard turning. J Manuf Sci Eng 128(1):104–109
23. Huang Y, Liang S (2004) Modeling of CBN tool flank wear progression in finish hard turning. J Manuf Sci Eng 126(1):98–106
24. Kümmel J, Braun D, Gibmeier J, Schneider J, Greiner C, Schulze V, Wanner A (2015) Study on micro texturing of uncoated cemented carbide cutting tools for wear improvement and built-up edge stabilization. J Mater Process Technol 215:62–70
25. Cheng K, Luo X, Ward R, Holt R (2003) *Modeling and simulation of the tool wear in nanometric cutting*. Wear **255**(7–12):1427–1432
26. Su H, Liu P, Fu Y, Xu J (2012) Tool life and surface integrity in high-speed milling of titanium alloy TA15 with PCD/PCBN tools. Chin J Aeronaut 25(5):784–790
27. Cheng K (2008) Machining dynamics: fundamentals. In: applications and practices, vol 2008. Springer, London, November
28. Altintas Y (2012) Manufacturing automation: metal cutting mechanics, machine tool vibrations, and CNC design, 2nd Edition: Cambridge university press.
29. Archard J (1953) Contact and rubbing of flat surfaces. J Appl Phys 24(8):981–988
30. Wang J, Zheng C (2002) An analytical force model with shearing and ploughing mechanisms for end milling. Int J Mach Tools Manuf 42(7):761–771
31. Wang J, Zheng CM (2002) Identification of shearing and ploughing cutting constants from average forces in ball-end milling. Int J Mach Tools Manuf 42(6):695–705
32. Carolan D, Ivanković A, Murphy N (2013) A combined experimental–numerical investigation of fracture of polycrystalline cubic boron nitride. Eng Fract Mech 99:101–117
33. Rahim M, Li G, Ding S, Mo J, Brandt M (2015) Electrical discharge grinding versus abrasive grinding in polycrystalline diamond machining—tool quality and performance analysis. Int J Adv Manuf Technol:1–15
34. Donachie M (2000) Titanium: a technical guide, 2nd Edition.: ASM international.
35. Oosthuizen E, Wang Z (2010) A review of the machinability of titanium alloys. R & D Journal of the South African Institution of. Mech Eng 26:43–52
36. Li G, Rahim M, Ding S, Sun S (2015) Performance and wear analysis of polycrystalline diamond (PCD) tools manufactured with different methods in turning titanium alloy Ti-6Al-4 V. Int J Adv Manuf Technol:1–17
37. D. McNamara, D. Carolan, P. Alveen, N. Murphy, A. Invakovic, Effect of loading rate on the fracture toughness and failure mechanisms of polycrystalline diamond (PCD). International Journal of Refractory Metals and Hard Materials, 2016. 60: p. 1–10.
38. Bai Q, Yao YX, Bex P, Zhang G (2004) Study on wear mechanisms and grain effects of PCD tool in machining laminated flooring. Int J Refract Met Hard Mater 22(2):111–115
39. Sun S, Brandt M, and Dargusch M (2015) Effect of tool wear on chip formation during dry machining of Ti-6Al-4V alloy, part 1: effect of gradual tool wear evolution. Proceedings of the Institution of Mechanical Engineers, Part B: Journal of Engineering Manufacture, p. 0954405415599956.